Journal of Cleaner Production 368 (2022) 133143

Contents lists available at ScienceDirect

Journal of Cleaner Production

journal homepage: www.elsevier.com/locate/jclepro

Towards sustainable production of minerals and chemicals through seawater brine treatment using Eutectic freeze crystallization and Electrodialysis with bipolar membranes

A. Culcasi [a], R. Ktori [b], A. Pellegrino [a], M. Rodriguez-Pascual [b], M.C.M. van Loosdrecht [b], A. Tamburini [a], A. Cipollina [a,*], D. Xevgenos [b,**], G. Micale [a]

[a] Dipartimento di Ingegneria, Università di Palermo (UNIPA)-Viale delle Scienze ed. 6, 90128, Palermo, Italy
[b] Department of Biotechnology, Delft University of Technology, Delft, the Netherlands

ARTICLE INFO

Handling Editor: Prof. Jiri Jaromir Klemeš

Keywords:
Circular economy
Ion exchange membrane
ZLD
Brine management
EFC
BMED

ABSTRACT

European policy encourages the adoption of sustainable systems that promote the efficient use and recovery of minerals and chemicals. In this respect, desalination brines do contain a dramatic amount of valuable minerals and can be valorized through appropriate treatments rather than releasing them into the environment. This paper proposes an innovative brine recovery system for obtaining high purity chemicals through the integration of *Eutectic Freeze Crystallization* (EFC) and *Electrodialysis with Bipolar Membrane* (EDBM) technologies. Two separate laboratory-scale experimental campaigns were carried out to validate the potential integration of the two processes. Mirabilite ($Na_2SO_4 \bullet 10H_2O$) has been recovered with a purity of 99.9% using the EFC, and a feed rich in NaCl with low impurities has been further processed in an EDBM unit. EDBM tests with feed solutions simulating EFC effluents have shown that it is possible to produce acidic and basic solutions with high purity (>99%), despite the presence of impurities in the feed. Interestingly, the low EDBM specific consumptions of 0.9–1.1 kWh kg_{NaOH}^{-1} at 100 A m^{-2} and 1.3–1.6 kWh kg_{NaOH}^{-1} at 300 A m^{-2} were comparable with and without impurities. In the context of the circular economy strategy promoted by the EU-H2020 Water Mining project, the current study demonstrates that this integrated system effectively minimizes waste, promoting sustainability while providing a potential economic return.

1. Introduction

Freshwater scarcity is one of the world's greatest challenges, endangering economic growth, social security, and ecosystem health (Tong and Elimelech, 2016). A possible solution to ensure adequate water supply is seawater desalination (Panagopoulos et al., 2019). Indeed, according to projections, the desalination industry will produce approximately 54 billion m^3 of water per year by 2030 (Shahzad et al., 2017). Aside from freshwater, desalination technologies also produce a concentrated wastewater stream, known as brine (Molinari et al., 2021), which is typically disposed of using methods such as sewer discharge, deep-well injection, surface water discharge, and evaporation ponds (Panagopoulos and Haralambous, 2020a, Xevgenos et al., 2015a). However, these brines also represent an incredibly rich source of valuable elements, whose recovery could be economically viable and environmentally sustainable, as it could contribute reducing the risk of negative environmental impacts due to the disposal of such concentrated brines (Panagopoulos and Haralambous, 2020b).

In March 2020, as part of the European Green Deal, the European Commission adopted a new circular economy action plan (CEAP). Specifically, wastewater recycling and reuse is a promising solution that can be achieved using Zero Liquid Discharge (ZLD) or Minimum Liquid Discharge (MLD) approaches, enabling the EU targets to be met (Panagopoulos and Haralambous, 2020a). The ZLD approach utilizes of a variety of desalination methods to generate freshwater and eliminate all liquid waste (Xevgenos et al., 2015b). On the other hand, the MLD approach is similar to ZLD in that it employs similar technologies, but they are integrated to recover up to 95% freshwater (Panagopoulos and Haralambous, 2020a). Pre-treatment and pre-concentration steps are both included in the ZLD and MLD approaches. Particularly, gravity settling and filtration for settleable solids are common pre-treatment

* Corresponding author.
** Corresponding author.
E-mail addresses: andrea.cipollina@unipa.it (A. Cipollina), d.xevgenos@tudelft.nl (D. Xevgenos).

https://doi.org/10.1016/j.jclepro.2022.133143
Received 24 December 2021; Received in revised form 11 June 2022; Accepted 12 July 2022
Available online 15 July 2022

Nomenclature

Symbols

$Amax$ (mm^2)	biggest crystal mean size
C (mol l^{-1})	molar concentration
F (C mol^{-1})	Faraday constant
G (mm^2 min^{-1})	growth rate of the crystals
I (A)	applied current at the external generator
M (g mol^{-1})	molar mass
$m_{IN,\ Na_2SO_4}$ (g)	total Na2SO4 mass ingoing to the EFC
$m_{OUT,\ Na_2SO_4}$ (g)	total Na2SO4 mass outgoing from the EFC
N (−)	number of triplets
R (−)	recovery of sodium sulphate in the EFC
SEC (kWh $kg^{-1}_{\ NaOH}$)	Specific Energy Consumption per kg of NaOH
SP (kg m^{-2} y^{-1})	Specific productivity
t (s)	process time of the EDBM experiments
t_c (min)	process time of the EFC experiments
U (V)	applied potential at the external generator
U_{salt}	saturation of solution
V (l)	generic volume

Greek letters

η_{c,OH^-} (−)	OH- current efficiency
τ_{NaOH} (−)	NaOH yield

Acronyms/abbreviations

AEM	Anion-Exchange Membrane
BPM	Bipolar Membrane
CEAP	Circular Economy Action Plan
CEM	Cation-Exchange Membrane
CSD	Crystal Size Distribution
CFD	Computational Fluid Dynamics
DC	Direct Current
DSA	Dimensionally Stable Anode
EDBM	ElectroDialysis with Bipolar Membranes
EFC	Eutectic Freeze Crystallizer
EP	Eutectic Point
ERS	Electrode Rinse Solution
EU	European Union
GHG	GreenHouse Gas
IEM	Ion Exchange Membrane
LCoNaOH	Levelized Cost of NaOH
MED	Multi Effect Distillation
MF-PFR	Multiple Feed – Plug Flow Reactor
MLD	Minimum Liquid Discharge
OP	Operating Point
OT	Operating Temperature
RO	Reverse Osmosis
SEC	Specific Energy Consumption
ZLD	Zero Liquid Discharge

steps, as well as pH adjustments (Prihasto et al., 2009), nanofiltration (Micari et al., 2020), and chemical precipitation (Semblante et al., 2018). Importantly, these pre-treatment steps also include membrane cleaning, which is critical for improving membrane performance and extending the life of the process but necessitates the use of chemicals such as hydrochloric acid (Madaeni and Mansourpanah, 2004). The most common pre-concentration steps include reverse osmosis (Tong and Elimelech, 2016), forward osmosis (Ahmed et al., 2019), and electrodialysis (Campione et al., 2018). However, in the case of the ZLD, the treatment also includes evaporation and crystallization steps, in order to achieve total freshwater recovery and zero liquid waste. Multi Effect Distillation (MED) (Ma et al., 2021) is the most frequently used evaporation process, while brine crystallization (Lassesson et al., 2021; Xevgenos et al., 2015b) is a popular method for salt mixture recovery. However, the salts gathered in this manner have no market value and must be treated as waste, incurring management and disposal costs.

Few studies in the literature have aimed to selectively recover resources that would otherwise be lost by waste brines, such as chlorides and sulphates in the form of sodium, magnesium, and calcium salts. Indeed, despite the fact that the proposed treatments are designed to reduce liquid effluents, they nonetheless result in the generation of liquid streams of brine containing high species concentrations, which may alter the ecosystem if disposed back to the sea (Xevgenos et al., 2021; Avramidi et al., 2022). An understudied alternative crystallization process is Eutectic Freeze Crystallization (EFC), which is capable of separating aqueous solutions into water ice and pure solidified solutes (Randall and Nathoo, 2018). In general, treatment chains that use ZLD approaches consume more energy due to the high energy costs of evaporative steps (e.g., MED) and crystallization. Indeed, while the pre-concentration steps (i.e., membrane-based) fall within the range of 0–20 kWh m^{-3} of produced water, the evaporation and crystallization steps fall within the range of 10 to more than 70 kWh m^{-3} of produced water (Panagopoulos and Haralambous, 2020b). It is clear that the ZLD strategy, while capable of reducing liquid waste, entails significant investment capital and energy costs (i.e., 4–5 times higher). The cost of energy is directly reflected as a cost for the environment, specifically in terms of the amount of greenhouse gas (GHG) emissions. Regarding CO_2 emissions, considering an average value of 0.47 kg CO_2 per kWh (Micari et al., 2020), membrane-based processes emit approximately 4.7 kg CO_2 m^{-3} of produced water, while thermal processes may emit 33 kg CO_2 m^{-3} of produced water. The potential production of salts from the brine can give an economic return that ranges from $100 to $300 per ton (Panagopoulos, 2020) and can improve the process feasibility, but, likewise, the systems used should be as energy efficient as possible in order to minimize emissions (Tsalidis et al., 2022).

Only a few of the proposed treatment chains are aimed at the production of chemicals and often generate waste streams that reduce the process's applicability (Du et al., 2018). Electrodialysis with bipolar membranes (EDBM) is an electro-membrane technology that can produce acids and bases from a waste saline solution (Culcasi et al., 2022). Compared to traditional ZLD systems, the integration of EDBM technology could lead to advanced brine chemical recovery systems that provide a significant economic return from the treatment chain and improve its sustainability. EDBM has the potential for the in-situ production of chemical reagents required by the treatment chain, such as acid solutions for membrane cleaning pre-treatments and alkaline solutions for both reactive crystallization and the possible pH adjustment of output currents.

In this study, EFC and EDBM are proposed for a synergic integration, which can be strategically combined with other existing technologies to bring the concept of a zero-waste process closer to reality (Randall et al., 2011). Unlike previous research, this work aims to selectively recover multiple high-purity products rather than removing or rejecting them and to produce a solid waste mixture. Water and sodium sulphate are recovered from EFC, while EDBM yields highly pure NaOH and HCl solutions, eventually minimizing the concentration of the salty solution leaving the treatment chain, while concurrently producing chemicals useful to the industry. These chemicals, along with the produced sodium sulphate and water, add significant value to the system, thus making it economically competitive. In this way, resource circularity is ensured, and environmental sustainability is maximized.

This research is part of the EU-funded WATER-MINING project. The WATER-MINING project aims to develop a seawater brine valorization treatment chain that maximizes freshwater and brine resource recovery

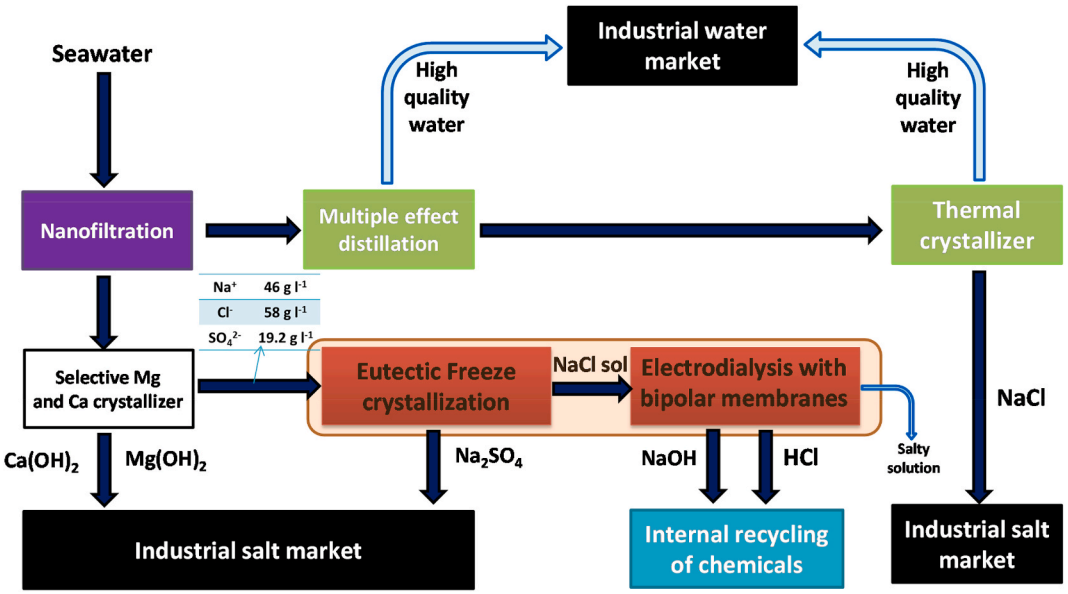

Fig. 1. The WATER MINING treatment chain.

(Fig. 1).

The current work focuses on the EFC and EDBM units, part of the larger WATER-MINING treatment chain (Petrik et al., 2022).

1.1. EFC description

Eutectic Freeze Crystallization (EFC) is an alternative technology capable of separating aqueous solutions into water and pure salts. EFC is a combination of melt crystallization (solvent crystallization) and cooling crystallization (solute crystallization) processes driven by temperature decrease. The basic principle of this process can be described using a phase diagram of a binary sodium sulphate (Na_2SO_4) - water mixture (Fig. 2).

For a system with concentration of salt lower than Eutectic Point (EP) concentration, the unsaturated solution (point A) is slowly cooled down until the solution becomes supersaturated for water. After metastability is broken at point B, ice crystals are formed, and further cooling brings the solution to EP where salt crystals begin to form. In the case of a system with a higher concentration than the EP, salt will form first, followed by ice. At the EP, ice, mother liquid at the eutectic concentration, and salt ($Na_2SO_4 \bullet 10H_2O$ in this study) are in equilibrium. In order to maintain supersaturation, and therefore continue the crystallization of ice and salt, the Operating Point (OP) and therefore the Operating Temperature (OT) is lower than the EP (and the Eutectic Temperature (ET)) of the system. This difference in temperature between EP and OP is the crystallizing driving force, and responsible for the nucleation, growth and production rate. Gravitational separation of ice and salt is an added advantage of Eutectic Freeze Crystallization because of the solution, ice, and salt difference in density. In particular, salt sinks to the bottom of the crystallizer while ice floats to the top (Randall et al., 2011). Eutectic Freeze Crystallization is increasingly gaining interest as a brine treatment solution since EFC requires less energy to recover water and salts from brine compared with other thermal processes (the latent heat of fusion of ice is about six times lower than the latent heat of vaporization of water) (Heydenrych et al., 2018). EFC can be used as the final step after any process where hypersaline water/brine is produced. Various studies have assessed the application of EFC to treat RO brine from mining industry (Randall et al., 2011) and textile industry (Randall et al., 2014), to treat cation exchange spent regenerant (Salvador Cob et al., 2014).

Depending on the solubilities and concentrations of the solute components, EFC is capable to selectively recover salts and concentrate the

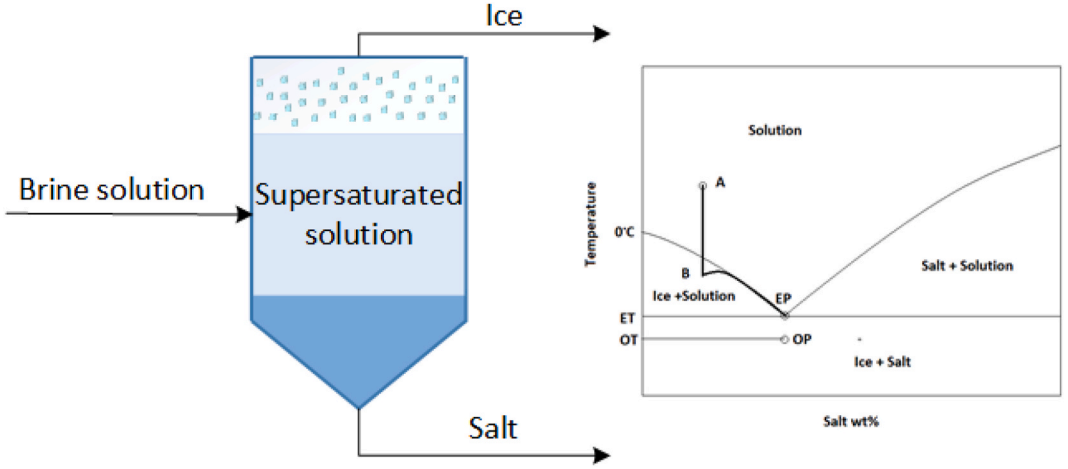

Fig. 2. Left: Simplified representation of the eutectic freeze crystallization process. Right: Thermodynamic phase diagram of the process. A: initial solution, B: same solution composition as in A in the "Ice + Solution" phase region, OT: Operating Temperature, OP: Operating Point, EP: Eutectic Point, ET: Eutectic Temperature.

feed solution by removing ice. In this work, EFC is used to recover the maximum amount of sodium sulphate (Na_2SO_4) without crystallizing NaCl, thus producing Na_2SO_4 salt and a concentrated stream of NaCl. The selective crystallization can be achieved in this case because NaCl is undersaturated in comparison to Na_2SO_4, at this OP temperature and concentration.

In the present work, EFC is used to treat the brine stream from seawater already pretreated by nanofiltration and selective precipitation (see Fig. 1) to remove Mg $^{2+}$ and Ca $^{2+}$. The feed stream to the EFC Crystallizer consists mainly of a ternary system of Na^+, Cl^-, SO_4^{2-} and some minor impurities (e.g., K^+). This system is similar to that reported by Reddy et al. (2010) and its thermodynamics can be represented by the experimental data of the ternary phase diagram reported by Wang et al. (2018). The effect of impurities on the eutectic point will be assessed in the present study.

1.2. EDBM description

EDBM dissociates water molecules into proton and hydroxide ions, thus allowing the production of acidic and alkaline solutions. EDBM is an eco-friendly way to make acid and base solutions (Huang and Xu, 2006). Firstly, the EDBM does not require rare or precious materials. Indeed, the electrodes can be made from a sustainable carbon source, rather than expensive metals. Also, all materials used can be recycled, reducing waste production at the end of the unit's life. Secondly, the EDBM improves safety. For example, no toxic materials are used in this technology, and the risk of a fire or explosion is minimal. Thirdly, the EDBM is highly scalable and has a low Specific Energy Consumption (SEC) for both acid and base production. The working principle and set-up of the EDBM unit is depicted in Fig. 3.

The EDBM unit is a stack including many repetitive units called triplets (Fig. 3) and made up of one cationic, one anionic and one bipolar exchange membranes (i.e., CEM, AEM, and BPM, respectively) with three interposed channels (i.e., salt, acid, and base channels), which are typically created by the net spacers separating the membranes.

Within this setup, the Ion-Exchange Membranes (IEMs) act as barriers that selectively allow the passage of counter-ions while rejecting co-ions due to the effect of the so-called "Donnan exclusion principle" (Galama et al., 2013). EDBM stacks typically have a plate-and-frame configuration, where the repetitive units are piled one next to the other between two end-plates containing the electrodes. An external DC electric generator establishes an electron flux through the external electric circuit. The end-plates are in contact with the Electrode Rinse Solution (ERS), thus allowing electrons to transfer from the electrodes to the ionic species in solution by suitable redox reactions. The applied electric field drives the ionic current through the stack where cations migrate towards the cathode whilst anions migrate towards the anode.

Usually, salty water (e.g., NaCl solution) is pumped to the salt compartment whilst freshwater is pumped to the acid and base compartments. In general, the inlet concentration of the salty stream is determined by the desired concentration of NaOH or HCl.

When the water dissociation potential is reached, the dissociation of the water molecules begins. This reaction occurs within the interlayer of the bipolar membranes and, because of this reaction, proton ions will be produced on one side of the bipolar membrane, and hydroxide ions will be produced on the other side. Simultaneously, the salt ions are driven to opposite sides in the salt channel depending on their charge due to the applied electric field. As a result, at the outlets, a diluted salt is obtained in the salt channel, hydrochloric acid in the acid channel and sodium hydroxide in the base channel.

The conversion and recovery of hypersaline industrial wastewaters is one of the important industries where EDBM can be applied (Herrero-Gonzalez et al., 2020). In this regard, many works have been devoted to demonstrating the application of EDBM to the desalination industry. EDBM might be used to obtain hydrochloric acid and sodium hydroxide solutions from desalination seawater brine.

The aim of this study was to investigate the integration of EFC and EDBM technologies for the valorization of seawater brines to recover salt and chemicals. To achieve this aim two experimental studies were conducted to assess the benefits of integrating the two technologies by evaluating the main performance indicators across varying process conditions. A multi-component feed simulating real brines was utilized to ensure the applicability of the results to the real-world use of this technology for desalination processes.

2. Material and methods

Two parallel experimental campaigns were conducted to study both EFC and EDBM. Here in after, the two test-rigs set-up will be described.

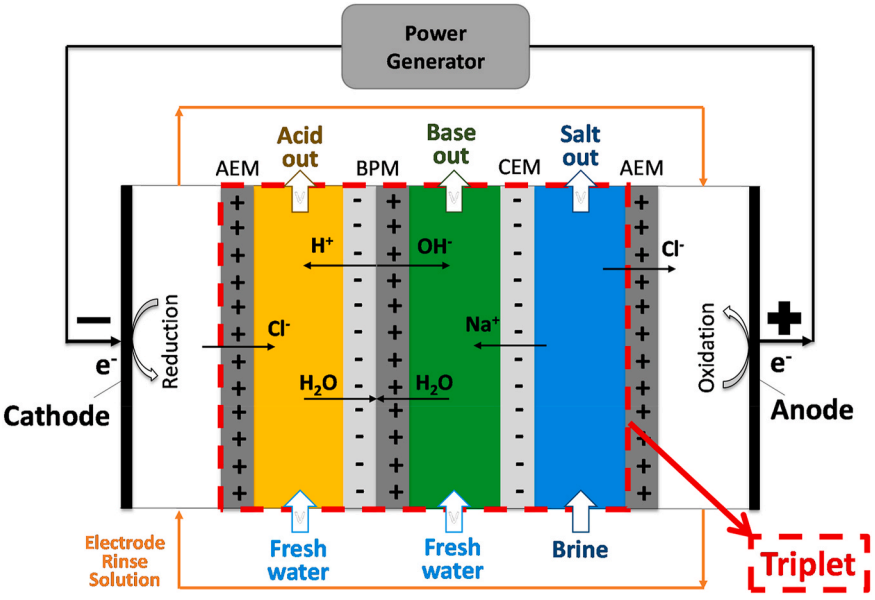

Fig. 3. Schematic of an ElectroDialysis with Bipolar Membranes (EDBM) unit.

2.1. Lab-scale EFC set-up

The objectives of this experimental work were to: (i) characterize the performance of the system, (ii) maximize the recovery of Na_2SO_4 without crystallizing the NaCl salt (present in the mixture), and (iii) recover Na_2SO_4 crystals and ice of high purity.

For the experimental set-up (Fig. 4), a 5L triple-wall, cylindrical glass vessel was used, equipped with an anchor-shaped scraper. For the cooling of the crystallizer, a LAUDA RP 4090 CW cooling bath was used and Kryo90 was used as cooling liquid. The temperature inside the reactor was measured with the PT-100 probe connected to the bath. The temperature of the system could be monitored and controlled through the LAUDA Wintherm Plus thermostat control software. A Hei-TORQUE Precision 400 motor was connected to the scraper rotating axis, allowing measurement of torque up to 400 Ncm and a speed range between 10 and 2,000 rpm. The ice and salt products were recovered after washing and filtration. Fig. 4 shows the scheme of the experimental EFC setup.

EFC is used to treat the brine stream free from Mg^{2+} and Ca^{2+} through suitable pre-treatment (nanofiltration and selective crystallizer). A synthetic feed solution mimicking the concentrate stream coming from the Multiple Feed – Plug Flow Reactor (MF-PFR) was prepared and transferred to the 5L EFC setup. For the synthetic mixture, 5L of ultra pure water was used with addition of 6.9 wt% NaCl, 3.8 wt% Na_2SO_4 and 2.4 wt% KCl.

The temperature of the cooling liquid was maintained at −5 °C. Then it was gradually decreased by 1 °C to maintain the temperature difference between the cooling liquid and the reactant solution less than 2.5 °C, until the system reached eutectic conditions. It is important to keep low the temperature difference between the cooling liquid and the reactant solution to avoid ice scaling on the wall and ensure the heat transfer in the system. After reaching eutectic conditions, the supersaturation was maintained to keep producing ice and salt crystals until the solid content in the crystallizer exceeded the limit to allow gravitational separation.

Filtered samples were taken every approximately 2 °C. Pictures of the crystals were taken to analyze the crystallization rate and the size distribution. A Dino-Lite Digital Microscope and a white light source were used for image acquisition through DinoCapture 2.0 software. ImageJ software was used for the analysis of the images and for generating crystal size distributions.

Salt was filtered out and washed with saturated Na_2SO_4 solution to eliminate the mother liquid around the crystals and evaluate the uptaken of impurities inside the $Na_2SO_4 \bullet 10H_2O$ crystals. The effect of washing on the purity of the products was also assessed and for this reason the washing procedure was repeated two times. The washing procedure was also performed for ice using ultra pure water (at 0 °C) to get rid of the mother liquid around the ice crystals, to evaluate the effect of washing the uptake of impurities around ice crystals. After the filtration and washing step, the three streams (i.e., salt, ice, NaCl solution) were collected and weighed. Samples of liquid effluent, ice (recovered water), and salt were taken and analyzed. For the elementary analysis, an Ion Chromatography (IC) was used.

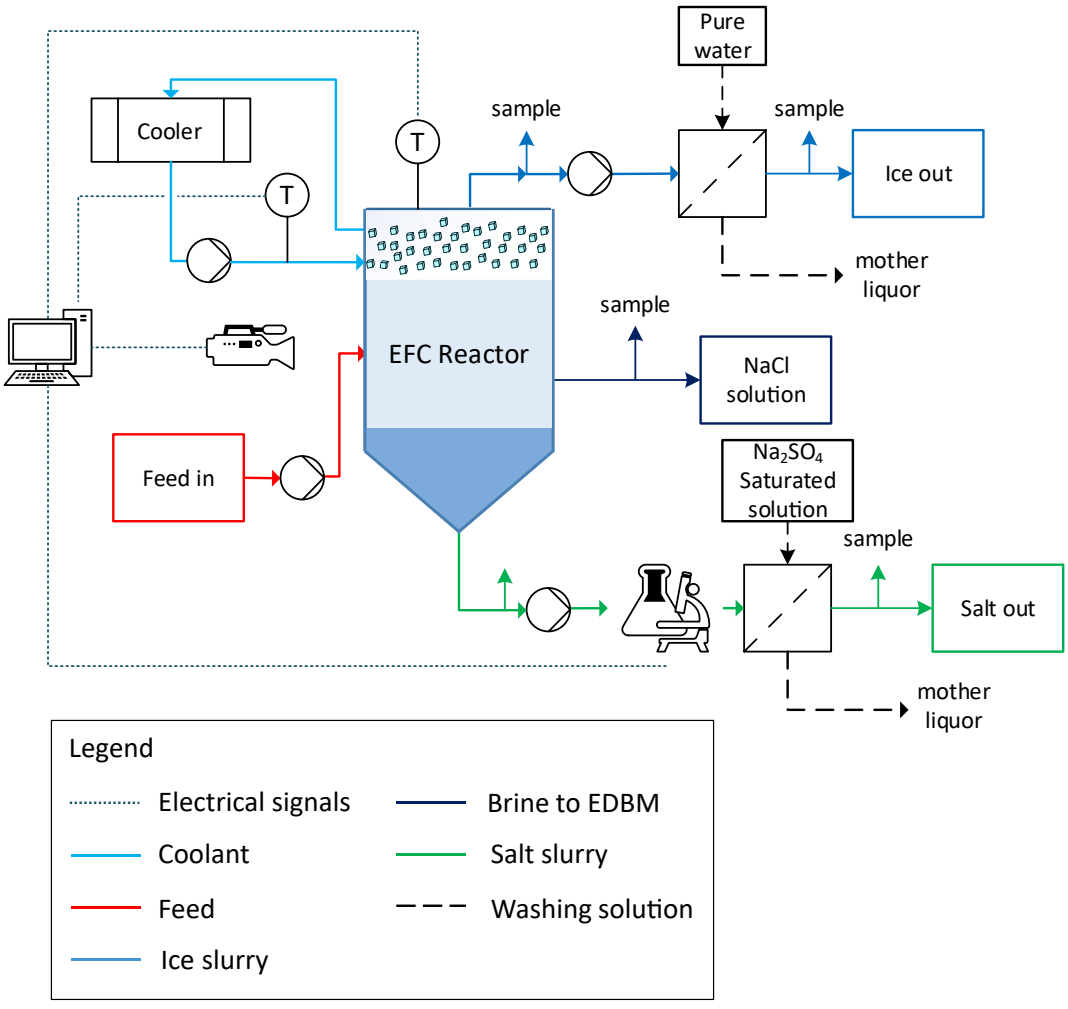

Fig. 4. Scheme of the experimental EFC setup.

2.2. Lab-scale EDBM set-up

The objectives of this experimental campaign were to: (i) analyze the effect of various feed compositions and concentrations on EDBM performance while simulating the presence or absence of EFC as pretreatment and (ii) evaluate the effect of various applied current densities, both in open-loop and closed-loop (batch) operating modes.

The experimental set-up (Fig. 5) included an EDBM unit (FT-ED-100, sourced from Fumatech BWT Gmbh, Germany) provided with commercial ion-exchange membranes; fumasep® FAB as AEM, fumasep® FKB as CEM, and fumasep® FBM as BPM.

The stack was assembled with 5 repeating units. The active area of the membrane was 10 × 10 cm^2 and channels were formed between each of the membranes using PVC/ECTFE woven spacers 480 μm thick. There were three inlet/outlet holes in the spacers for each channel, and these holes each had a diameter of 8.5 mm. The system had a cross-flow arrangement. In order to convert the electrons flux in the external circuit into an ionic current, the system is equipped with two Dimensionally Stable Anode (DSA) type electrodes in the final compartments. The feed solutions were prepared with demineralized water, including specifically NaCl (99.7% ChemSolute), Na_2SO_4 (99% Honeywell Fluka), HCl (37% Merck), and NaOH (98–100% Honeywell Fluka). For the electrode rinse, an aqueous solution was used with 0.5 M in $FeCl_2/FeCl_3$ (99% ChemSolute) and 0.6 M in HCl. Both steady-state and dynamic conditions were employed for this experimental campaign. Two types of tests, in particular, were performed. First, steady-state tests were conducted in a once-through (single pass) configuration. Second, dynamic tests in a closed-loop configuration were performed. Closed-loop tests involve recirculating electrolyte solutions in the same tank. Once-through tests consists of the passage of the electrolyte solutions from the inlet tanks to the outlet ones, without recirculation. Acid, base and salt solutions were fed into the channels with fluid velocities of 1 cm s^{-1} for all the tests, and this was done using peristaltic pumps (BT601S, Lead Fluid Technology, CO LTD, China). A hydraulic test was performed at the beginning of each test to ensure that there was no leakage and that there were no air bubbles in the stack or pipes.

All the experiments were carried out at room temperature being ~20 °C. For the EDBM tests, a BK Precision 1902 DC Power Supply was utilized in galvanostatic mode. In order to assess experiment's reliability, they were all replicated at least two times. Two Fluke 175 multimeters were used to measure the stack voltage and current. A WTW 3320 portable conductivity meter was used to measure the conductivity of all the solutions in the external tanks. The concentrations of the ions in solution were measured by taking samples from the external tanks with syringes and subsequently performing titrations and chromatographic analyses. Ion chromatography was performed by using an Ion Chromatography Metrohm 882 Compact IC plus.

Various compositions and concentrations of feed solutions were utilized. For all tests, the inlet salt solutions contained 2M NaCl and a variable concentration of Na_2SO_4 ranging from 0 to 0.5M. For the once-through tests, the inlet solutions of the acid and alkaline compartments were HCl/NaOH at concentrations of either 0.05M or 0.6M, while distilled water was used for the closed-loop tests.

Before each experiment, membranes were conditioned by letting the inlet solution to flow in the stack for at least 5 min. After conditioning, the external power supplier was turned on to provide the electric current. In once-through configuration tests, the power supplier continued until a constant external voltage was obtained (i.e., once the steady-state condition is reached). In closed-loop configuration tests, the dynamic experiment continued until a NaOH target concentration of 1M was reached.

2.3. Evaluation of EFC and EDBM performance

The results of the experimental campaigns were analyzed to determine the main performance parameters. These are described in this section for both the technologies examined in this work.

2.3.1. EFC performance parameters

The recovery (% R) of sodium sulphate in the EFC unit is calculated as the ratio of the mass of recovered sodium sulphate to the total inlet sodium sulphate entering the EFC. It is given by,

$$\%\ R = \frac{m_{OUT,\ Na_2SO_4}}{m_{IN,\ Na_2SO_4}} \times 100 \tag{1}$$

where $m_{IN,\ Na_2SO_4}$ is the total Na_2SO_4 mass ingoing to the EFC and $m_{OUT,\ Na_2SO_4}$ is the total Na_2SO_4 mass outgoing from the EFC in the form of salt. The recovered amount of Na_2SO_4 is calculated as the mass fraction of Na_2SO_4 in $Na_2SO_4 \bullet 10H_2O$ (i.e., mirabilite):

$$m_{OUT,\ Na_2SO_4} = m_{OUT,\ SALT} \times \frac{M_{Na_2SO_4}}{M_{Na_2SO_4 \cdot 10H_2O}} \tag{2}$$

where $M_{Na_2SO_4}$ and $M_{Na_2SO_4 \cdot 10H_2O}$ are the mole masses of Na_2SO_4 and $Na_2SO_4 \bullet 10H_2O$, respectively and $m_{OUT,\ SALT}$ is the total mass of salt exiting the EFC unit.

The purity of the salt and water is assessed as follows,

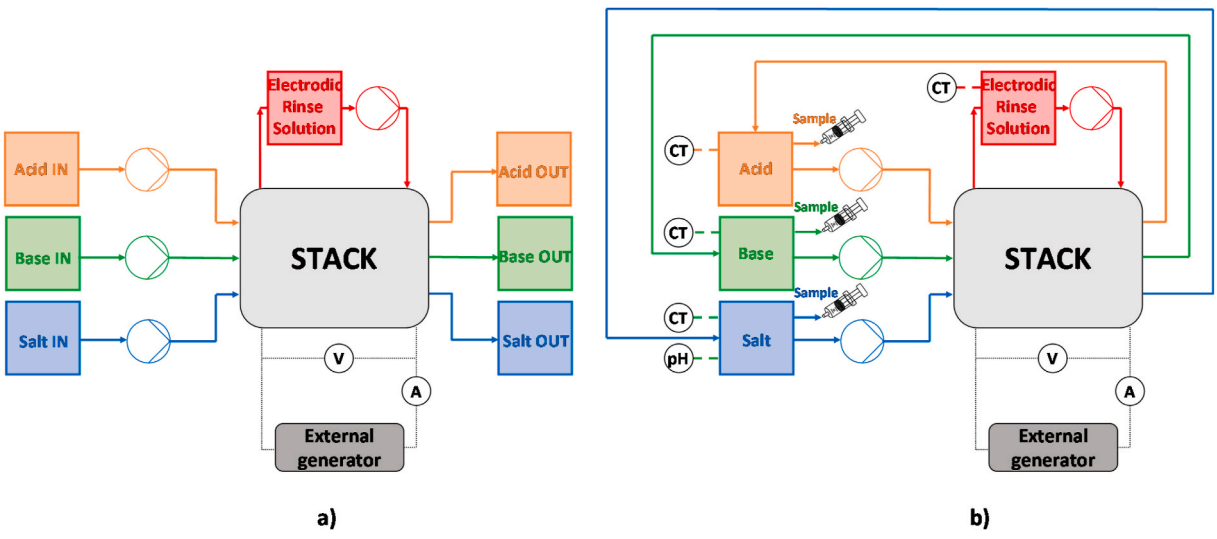

Fig. 5. Schemes of the experimental set-ups for a) once-through and b) closed-loop operations.

$$\%\ EFC\ productpurity = \left(1 - \frac{\sum_i^n Mi}{m_{OUT,\ product,}}\right) \times 100 \quad (3)$$

where Mi is the mass of impurity i in the product (salt or ice) and $m_{OUT,product}$ is the total mass of product outgoing from the EFC.

The saturation of the solution (U_{salt}) is calculated according to the Pitzer model (Nima Yazdanpanah, 2020) as follows,

$$U_{salt} = \frac{K}{K_0} \quad (4)$$

where K_0 is the solubility constant at equilibrium and K is the current solubility constant.

The growth rate G (mm^2 min^{-1}) is given by,

$$G = \frac{Amax}{t_c} \quad (5)$$

in which, $Amax$ (mm^2) is the ratio between the biggest crystal mean size, and the batch time t_c (min) (Becheleni et al., 2017).

2.3.2. EFC performance parameters

The current efficiency (η_c) of NaOH for the EDBM process is defined as the ratio of the equivalent amount of charge transported by OH^- to the total electrical charge, and it is given by

$$\eta_c = \frac{F\left(V_{b,t}\ C_{NaOH,t} - V_{b,0}\ C_{NaOH,0}\right)}{N\ I\ \Delta t} 100 \quad (6)$$

in which, F is the Faraday constant (96,485 C mol^{-1}), $V_{b,t}$ and $V_{b,0}$ are the solution volumes (l) in the base container at time t and at the beginning of the test, respectively, $C_{NaOH,t}$ and $C_{NaOH,0}$ are the NaOH concentrations (mol l^{-1}) in the base container at time t and at the beginning of the test, respectively, N is the number of triplets, I is the applied current (A) and Δt is the time difference between the end and the beginning of the test.

The Specific Energy Consumption (SEC) is the energy consumed by the EDBM process to produce 1 kg of NaOH. It is assessed as follows,

$$SEC = \frac{I \int_0^t U\ dt}{3,600\ M_{NaOH}\left(V_{b,t}\ C_{NaOH,t} - V_{b,0}\ C_{NaOH,0}\right)} = \frac{F \int_0^t U\ dt}{3,600\ M_{NaOH}\ N\ \Delta t\ \eta_c} \quad (7)$$

where U is the external voltage (V) and M_{NaOH} is the mole mass of sodium hydroxide (g mol^{-1}).

The yield of sodium hydroxide (τ) for the EDBM process represents the ratio of the produced sodium hydroxide moles to the initial sodium chloride. It is calculated as follows,

$$\tau = \frac{\left(V_{b,t}\ C_{NaOH,t} - V_{b,0}\ C_{NaOH,0}\right)}{V_{s,0}\ C_{NaCl,0}} \quad (8)$$

where $V_{s,0}$ is the solution volume of the salt container (l) and $C_{NaCl,0}$ is the NaCl concentration (mol l^{-1}) in the salt container at the beginning of the test.

The yearly Specific Productivity (SP) of the EDBM unit is calculated as follows,

$$SP = \frac{3.6\ M_{NaOH}\left(V_{b,t}\ C_{NaOH,t} - V_{b,0}\ C_{NaOH,0}\right) 8,000}{3\ N\ A_m\ \Delta t} \quad (9)$$

where A_m is the membrane active area (m^2).

Finally $\%\ SO_4^{2-}$ is the ratio between the moles of SO_4^{2-} ions and the total moles of anions present in the solution. It is calculated as,

$$\%\ SO_4^{2-} = \frac{n_{SO_4^{2-}}}{\sum_{anions} n_k} 100 \quad (10)$$

where $n_{SO_4^{2-}}$ is the SO_4^{2-} ion moles and n_k is the moles of the k-anion in the solution.

3. Results and discussion

In this section, the performance of the two technologies is examined, and a discussion of the benefits of their integration is presented.

3.1. EFC results

A synthetic solution of Na_2SO_4, NaCl, KCl, and water was used as feed in the 5 l EFC setup to evaluate the system's eutectic conditions, the recovery of Na_2SO_4 without crystallizing the present NaCl salt, and the purity of salt crystals and ice. KCl was added in order to determine the effect of impurities on the eutectic point of the understudy system.

The temperature profile of the reactant solution as a function of time is given in Fig. 6.

The system reached supersaturation and the first salt crystals were produced around 2.7 °C. NaCl in the feed solution increased the solubility of Na_2SO_4, decreasing the supersaturation of the solution and resulting in lower mirabilite nucleation temperature (Reddy et al., 2010). Therefore, the nucleation temperature for the ternary system was expected to be lower than 5 °C (Wang et al., 2018).

At the nucleation point, occurring after about 4 h, the first ice crystals were formed, and relevant latent heat was released. As a result, the solution temperature increased. Such peculiar behaviour can be explained thanks to the tendency of salty water solution undergoing metastable equilibria. In fact, in not seeded systems, the solution can go below the eutectic point keeping for a sustained time the metastable equilibrium (which was maintained, in our experiment, from about 2.5 to 4 h). Spontaneous nucleation only happened when this metastability was broken, thus generating a sudden formation of crystals and release of heat, that led to the temperature raise (from −5.8 °C up to −4.6 °C). Similarly, a peak due to the crystallization of salt is also visible around 0.5h, though much smaller than the one at 4 h, due to the much lower heat release of salts crystal formation.

Indeed, water (ice) has the property (or anomaly) that, compared with other substances, can be deeply in metastability, for example, down to −40 °C for pure water.

As the solution was further cooled, the salt production continued. This finding is consistent with the ternary diagram of the system NaCl–Na_2SO_4–H_2O and the experimental data from Wang et al. (2018), where the first eutectic conditions (Na_2SO_4•10$H_2$0 and ice) for their system were at −5.79 °C. This result indicates that the presence of NaCl affects the performance of the system, on the other hand, the effect of low KCl concentration is negligible.

One of the objectives of this experimental work was to maximize the

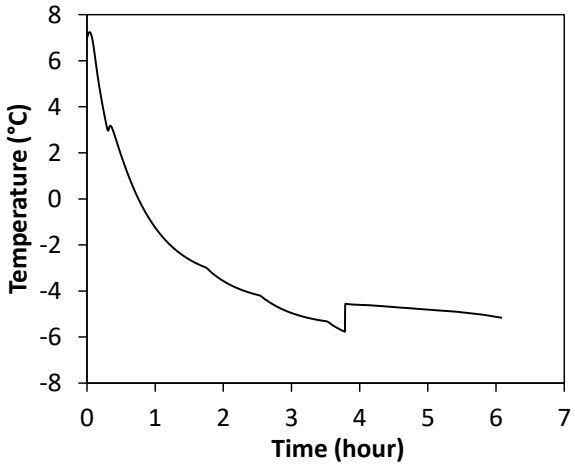

Fig. 6. Temperature profile of the feed solution.

recovery of Na_2SO_4 without crystallizing the NaCl salt. Fig. 7 shows the predicted salt solubilities in the understudy system calculated using the Pitzer model (Eq. (4)). When U_{salt} is lower than 1 the salt is undersaturated, when U_{salt} is equal to 1 it is saturated and when it is higher than 1 the salt is oversaturated (Nima Yazdanpanah, 2020).

It can be seen that mirabilite ($Na_2SO_4 \bullet 10H_2O$) starts to be supersaturated at ~5 °C, while hydrohalite ($NaCl \bullet 2H_2O$) is undersaturated in the whole temperature range in the understudy system. Therefore, the recovery of the sodium sulphate can be maximized without the crystallization of sodium chloride.

Filtered samples were taken every 2 °C approximately and they were analyzed. In Fig. 8, the ion concentration for the components is presented as a function of time (Fig. 8a) and temperature (Fig. 8b). As shown in Fig. 8, the concentration of the Na^+ and SO_4^{2-} were gradually decreased between 50 min and 3 h (between 2.7 °C and the eutectic temperature), which corresponded to the crystallization of $Na_2SO_4 \bullet 10H_2O$. In addition, Fig. 8 shows that only $Na_2SO_4 \bullet 10H_2O$ was crystallized and double salts were not found in the understudy system. After the eutectic point (time 3h and 35 min), where both salt and ice crystals were formed, the concentration of SO_4^{2-} remained approximately constant because the system tended to the thermodynamic equilibrium at the eutectic composition. The solution was still supersaturated in SO_4^{2-} ions, and thus $Na_2SO_4 \bullet 10H_2O$ and ice continued to crystallize. The concentration of the remaining ions was expected to increase because the water would have been removed from the solution in ice form. Since the change in temperature during the eutectic condition was small (see Fig. 6), and the production of salt and ice was high, the solid content in the crystallizer exceeded the limit to allow gravitational separation and the experiment was stopped. For this reason, the concentration of the remaining ions in Fig. 8 did not increase further after the experiment was stopped because there was no further ice crystallization.

In this study, the quality of salt crystals was assessed by performing the Crystal Size Distribution (CSD). Indeed, CSD influences the performance of the process and the separation of the crystals from the mother liquor (Lewis et al., 2015). Online image acquisition and post-processing analysis of the crystals during the crystallization process were used to evaluate the size distribution.

Fig. 9 shows images of the salt crystals obtained after 1 and 185 min of growth, which were used for CSD analysis and determining the growth rate.

The mirabilite crystals presented in Fig. 9 do not show any imperfections and therefore impurities were not uptaken into the crystal structure. Fig. 10 shows the difference in crystals size and population of crystals (% Frequency) between 1 min growth and 185 min growth.

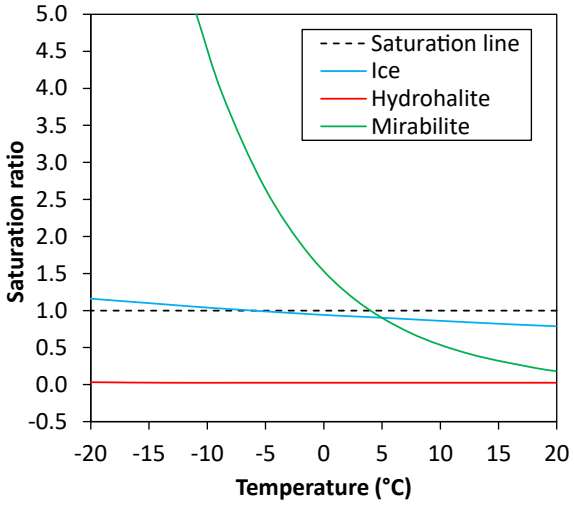

Fig. 7. Predicted salt solubilities in the understudy system.

The well faceted crystals are hexahedron in shape. The size distribution of the obtained salt crystals was measured using image analysis. ImageJ software was used for the analysis of the images and generate crystal size distribution. The size range was approximately 0–0.04 mm^2 after 1 min of growth. After 185 min of growth, the size range was approximately 0–0.16 mm^2. The CSDs showed a gradual increase in the mean salt crystal size as the crystallization time increased. The growth rate was determined using Eq. (5) as 0.0007 $mm^2\ min^{-1}$. In addition, it was estimated that the mean crystal size of salt crystals was 0.03 mm^2. It was found that 95.8% of the salt crystals increased in size after 185 min of growth. However, only a small fraction of the crystals had grown to sizes within the range of 0.11–0.16 mm^2 after 185 min of growth.

The effect of washing on the $Na_2SO_4 \bullet 10H_2O$ crystals to remove the mother liquid solution from the crystals' surface were assessed. The $Na_2SO_4 \bullet 10H_2O$ crystals were washed two times with a saturated solution of sodium sulphate. Samples of these solutions (one for each washing step) were analyzed to evaluate the effect of washing. Then, the salt crystals were diluted and then the samples were analyzed to evaluate if there were any impurities in the crystals. Table 1 shows the concentration of ions in the washed solutions after the two washing steps. The analysis showed that there was mother liquor on the surface of sodium sulphate crystals. The data show that 88.1% of the mother liquor that was on the surface of the crystals was removed after the first washing. Further washing removed 83.8% of the remaining mother liquor. The overall effect of the two washing steps is 98.1%, which resulted in a purer product. Table 1 also shows the ion concentration of the solution after salt crystals dilution with and without washing. From Table 1, it can be seen that the remaining amount of mother liquor around the salt crystals was negligible. The purity of the recovered $Na_2SO_4 \bullet 10H_2O$ crystals after washing procedure was 99.9%.

The effect of washing on the ice crystals and the removal of mother liquor from the ice crystals' surface was assessed. The ice crystals were washed two times with pure water to remove mother liquor from their surface and the ion concentrations of these solutions were analyzed. The ion composition of ice was analyzed to evaluate if there were any impurities in the crystals and determine the purity of the product. Table 2 shows the concentration of ions in unwashed ice, in ice after the second wash, and in the ice washed solutions.

The results showed that in total 52% of the mother liquor was removed from the surface of the ice by washing. The second washing removed 74% of the Cl^-, 81% of SO_4^{2-}, and 69% of the K^+. Further washing is required to remove further the mother liquor from the ice crystals' surface. In addition, the analysis of the ion concentration for the ice (i.e., after the 2 washes) showed that $Na_2SO_4 \bullet 10H_2O$ crystals and mother liquor were trapped in the ice crystals because even after the washing procedure, the concentration of Na^+, Cl^-, SO_4^{2-} were not negligible. The purity of the recovered water in form of ice was 93.3%. The current study focused on the recovery of high purity sodium sulphate rather than pure water recovery. Although the salt concentration of ice was lower than that of the initial solution, it cannot be considered pure water. Because there is still sodium sulphate in this solution, ice can be recirculated back into the treatment chain, and the cooling energy can be used to pre-cool the EFC feed solution. Another possibility is to sell the ice in the fishing industry.

The overall recovery of $Na_2SO_4 \bullet 10H_2O$ was calculated according to Eq. (1). The overall recovery of Na_2SO_4 was calculated using the amount of Na_2SO_4 in the initial solution and the mass of recovered salt. In the present study, the overall recovery was 71%. Better separation of salt crystals, liquid effluent, and ice can increase overall recovery and the purity of the products. The remaining concentrate NaCl solution was used as the EDBM unit's inlet stream. The concentration of this solution is given in Table 3.

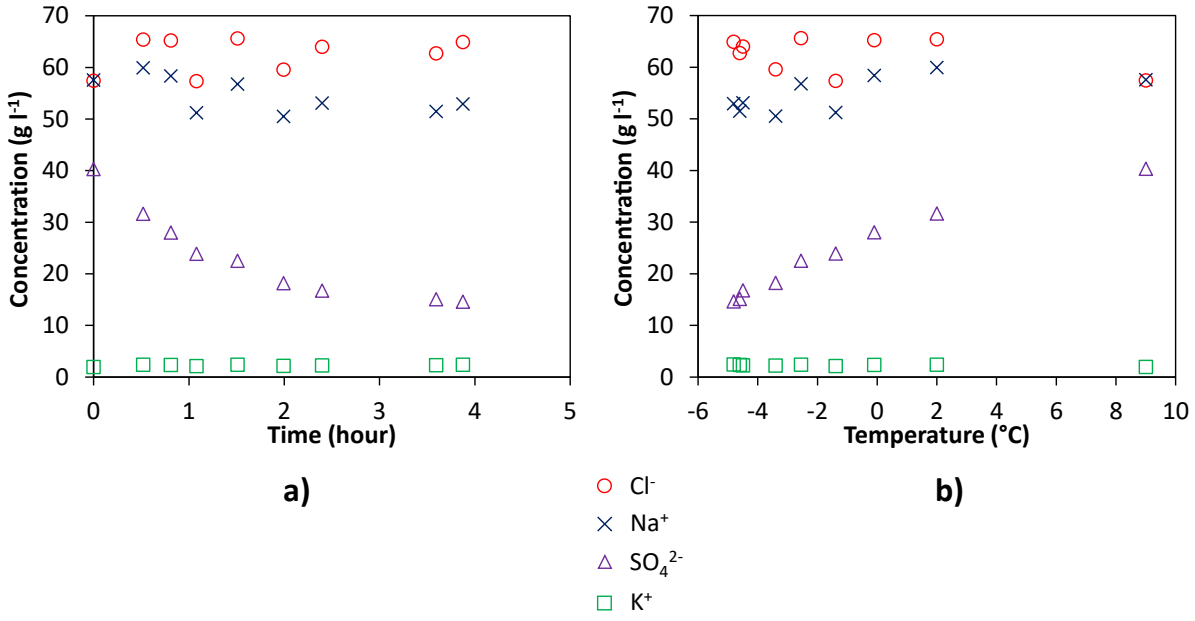

Fig. 8. Change in the concentration of ions in the solution inside the crystallizer as a function of a) time (hour) and b) temperature (°C).

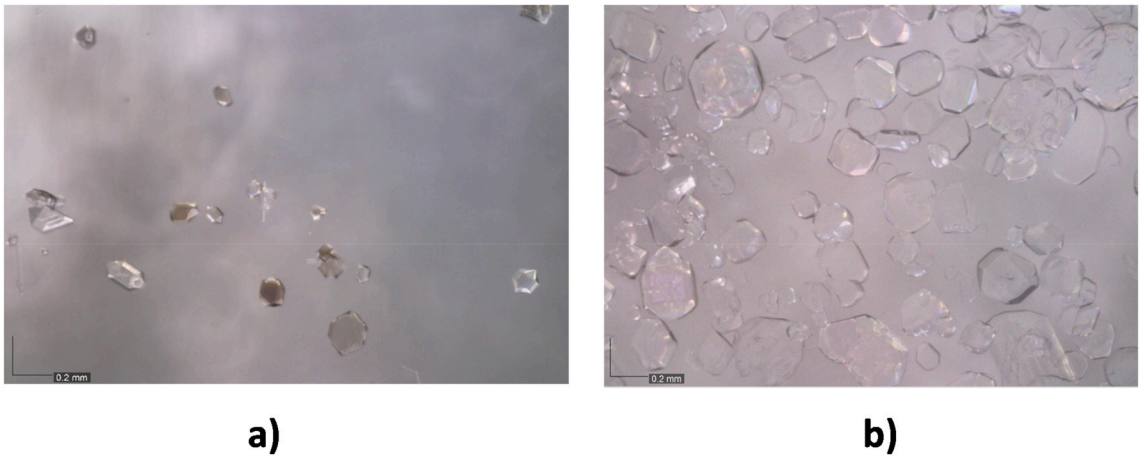

Fig. 9. Salt crystals after a) 1 min of growth and b) 185 min of growth.

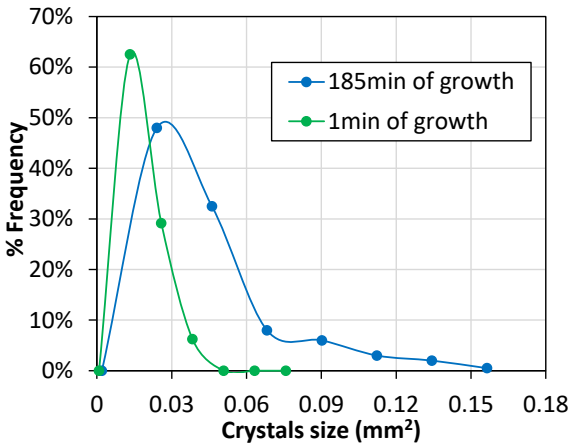

Fig. 10. Mirabilite CSDs obtained at 1 and 185 min of growth.

Table 1
Effect of washing on salt purity.

Solution description	Concentration (g l^{-1})				Salt purity
	Cl^-	SO_4^{2-}	Na^+	K^+	
Unwashed salt	8.5	140	78.3	0.0	93.7%
1 x washed salt[a]	1.0	167	90.3	0.0	99.3%
2 x washed salt[b]	0.2	195	108	0.0	99.9%
Outlet solution after 1st wash	8.3	46.8	32.0	0.1	–
Outlet solution after 2nd wash	0.5	48.5	28.9	0.0	–

[a] Ion concentration of solution after salt crystals dilution after the first wash with saturated solution.
[b] Ion concentration of solution after salt crystals dilution after the second wash with saturated solution.

3.2. EDBM results

Single-pass steady-state once-through tests were carried out to study the electrical behavior of the EDBM unit while varying the composition and concentrations of the feed solutions. Specifically, the polarization

Table 2
Effect of washing on ice purity.

Solution description	Concentration (g l^{-1})			
	Cl^-	SO_4^{2-}	Na^+	K^+
Unwashed ice	47.2	29.8	43.1	1.88
2 x washed ice[a]	22.9	20.1	23.5	0.890
Outlet solution after 1st wash	16.5	5.14	12.6	0.590
Outlet solution after 2nd wash	7.84	4.57	7.02	0.400

[a] Ion concentration of ice after the second wash with pure water.

Table 3
Salt concentration of the EFC liquid effluent and feed for EDBM unit.

Salt	Mass concentration (g l^{-1})	Molar concentration (mol l^{-1})
NaCl	92.3	1.58
Na_2SO_4	28.5	0.200
KCl	4.02	0.050

curves (i.e., current-voltage profiles) were obtained for different feeds. The aim was to conduct experimental simulations of the treatment chain for three different scenarios, namely A, B, and C. For experiments A, there was total recovery of Na_2SO_4 from the EFC (i.e., EDBM feed: 2M NaCl). Secondly, for experiments B, there was partial recovery of Na_2SO_4 from the EFC (i.e., EDBM feed: 2M NaCl and 0.1M Na_2SO_4). Finally, in experiments C the EFC was absent from the treatment chain (i.e., EDBM feed: 2M NaCl and 0.5M Na_2SO_4). Two different inlet concentrations of HCl and NaOH in the acid and alkaline compartments, respectively, were investigated for each experiment. The concentrations were either 0.05M or 0.6M, thus giving six different once-through experiments. The resulting polarization curves are shown in Fig. 11.

As demonstrated in Fig. 11a, there were negligible differences among the obtained polarization curves, regardless of the inlet acid and base concentrations utilized. Using the feed with 2M NaCl as reference, the average relative difference with the other curves was 4.4% when the inlet acid/base concentration was 0.05M. This was due to two major factors. Firstly, the ion salinity gradient had a negligible effect on the electromotive force across the monopolar membranes compared to the pH gradient across the bipolar membrane layers. Secondly, variations in the composition and concentration of the feed appeared to have no effect on the electrical resistance of the cell. Similarly, in the case of a higher inlet concentration of acid and base, equal to 0.6M, an average relative difference of 1.4% was observed (Fig. 11b). With the same applied current, the external voltage was different for the two acid and base concentrations. Particularly, as the concentrations increased, the average external voltage reduced. Indeed, this is the effect of two contrasting factors. Primarily, the increase in the inlet concentration of acid and base (from 0.05M to 0.6M) led to a rise in the Nernst potential (Culcasi et al., 2020), which leads to a higher minimum applied voltage in the second case; conversely, the increase in inlet concentration of acid and base resulted in the reduction of the stack electrical resistance, thus reducing the slope of the curve and leading to a lower final applied voltage.

Contrastingly, these results indicate that a very similar stack resistance (i.e., net resistance after subtracting the blank resistance) was obtained when varying the salt compartment composition and concentrations. Through calculating the stack resistance, it is possible to evaluate the resistance of the single repetitive unit when the blank resistance value is known. The latter was assessed through ad-hoc experiments conducted by assembling the stack with a single membrane (i.e., the end-membrane, in our case an AEM) and two spacers. When adopting an applied current density of 100 or 300 A m^{-2}, the measured blank resistance was 77 Ω cm^2 and 48 Ω cm^2, respectively. Subtracting the blank resistance from the stack resistance and dividing the result by the number of repetitive units enabled the apparent triplet resistance to be obtained. As a result, the triplet resistance was on average 32 Ω cm^2 and 20 Ω cm^2 for inlet concentrations of 0.05M and 0.6M, respectively. With 0.6M HCl and NaOH concentration, the resulting areal resistance was 37% lower compared to the value at 0.05M. The decrease in cell resistance was clearly due to a significant increase in the conductivity of the electrolytic solutions, especially in the presence of acids and bases. Having calculated all of these values, it is possible to approximately estimate the voltage that should be applied to the stack for a certain number of repetitive units. However, this estimation should be

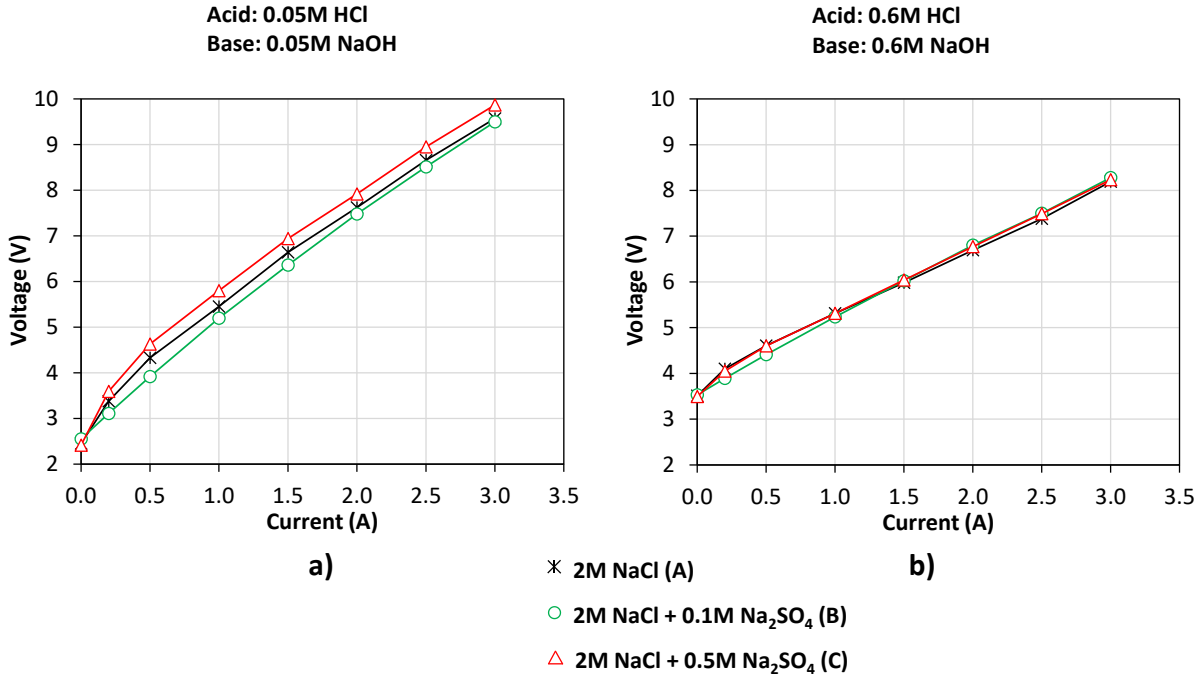

Fig. 11. Polarization curves as a function of the inlet concentrations in the three compartments, in once-through configuration. Inlet acid and base concentrations a) 0.05M and b) 0.6M.

interpreted carefully as the effect of parasitic currents through the manifolds are not taken into account, especially when using a high number of cells.

Tests were also conducted in closed-loop configuration. These enabled the evaluation of the EDBM unit performance with the aim of reaching 1M NaOH target concentration. The target was set in terms of NaOH concentration since this is the product with the highest commercial value. Once the target concentration was achieved, the tests were discontinued. The performance of the EDBM was determined in terms of NaOH concentration, SEC, current efficiency, and yield. In addition, these dynamic tests were carried out at two different current densities in order to study the possible discrepancies in performance. Fig. 12 shows the results obtained when applying a current density of 100 A m^{-2} for the three investigated scenarios. For the acid and base inputs, initial solutions of demineralized water were used (Culcaci et al., 2020a).

In these tests, the solution volumes were all 0.6 L. As follows from the stoichiometric relations in the water dissociation reaction, the maximum achievable NaOH concentration was greater than 1M. Therefore, the salt content in the feed was more than adequate to ensure the target was reached. Indeed, at the target concentration, the yield was equal to 50.5%, 45.8%, and 32.1% for scenarios A, B, and C, respectively. The reduction in yield in scenarios B and C predominantly resulted from the higher sodium ion content of the feed. The target concentration was reached in 318, 278, and 268 min for scenarios A, B, and C, respectively. Regarding the current efficiency, the recorded values for scenarios A, B, and C were 59.3%, 68.2%, and 71.4%, respectively. As is illustrated by Fig. 12c, the current efficiency showed a decreasing trend over time. The decreasing trend may be due to the significant impact of non-ideal detrimental phenomena, such as

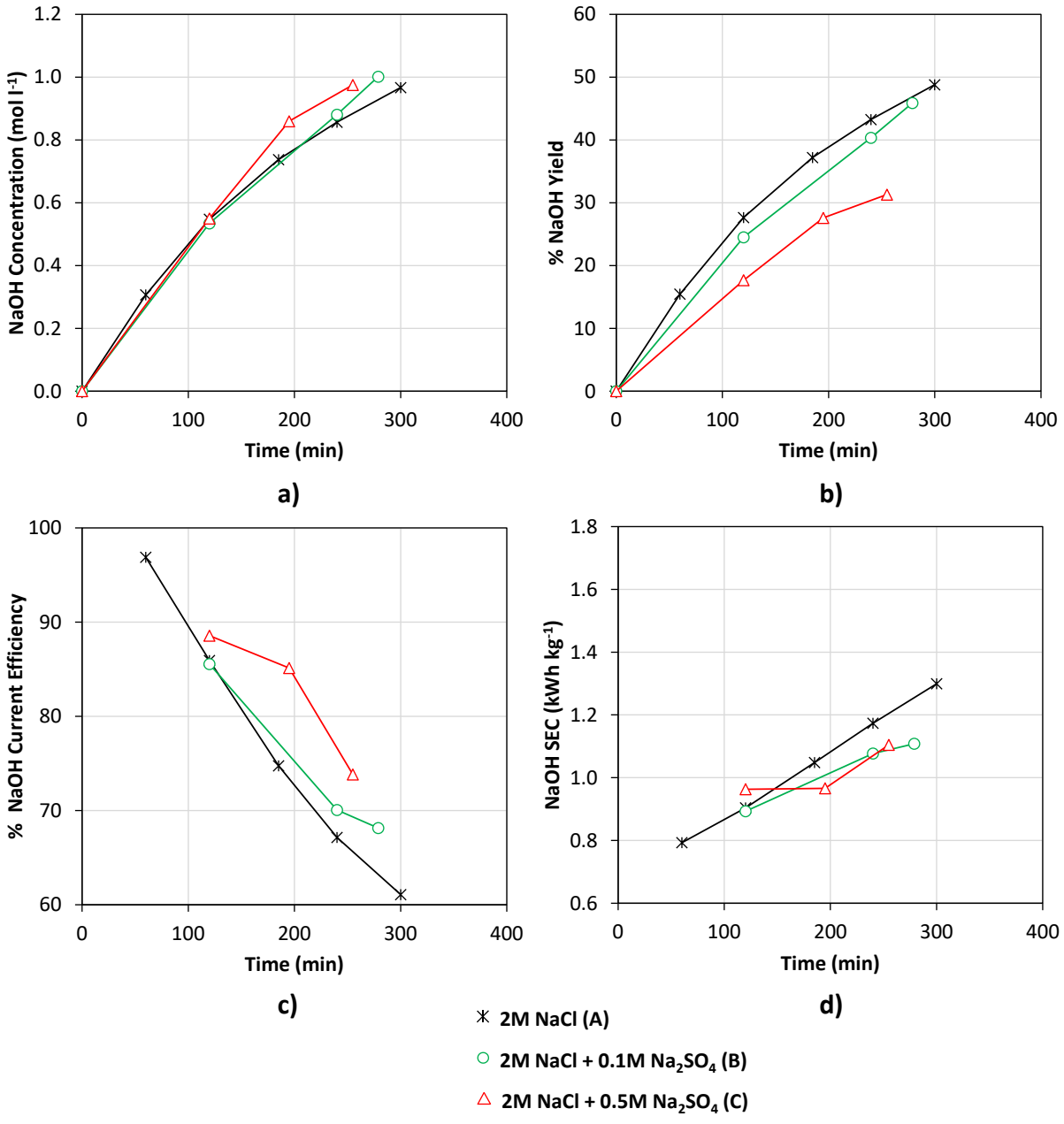

Fig. 12. Time dependency of a) Molar concentration of NaOH, (b) % Yield of NaOH (τ), (c) % Current efficiency of NaOH (η_c) and (d) Specific Energy Consumption of NaOH (*SEC*) as functions of time for a fixed current density of 100 A m^{-2} in a closed-loop configuration. Inlet acid/base compartments: demineralized water.

diffusion, osmosis, and electro-osmosis. By contrast, there was an increase in the specific consumption over time. The trend in the SEC (Fig. 12d) parallels that of the current efficiency, in line with the formula reported in section 2.3.2. Indeed, the SEC at the target was 1.34, 1.11, and 1.13 kWh kg^{-1}_{NaOH} for scenarios A, B, and C, respectively. Although the SEC is directly proportional to the external voltage applied (see Eq. (7)), the latter variable does not play a significant role in the SEC. Indeed, the voltage is relatively stable over time, which is in line with the graphs shown in Fig. 11 of the polarization curves.

In order to determine the potential annual production of the EDBM unit, the Specific Productivity value per total membrane area was evaluated. A value of 8,000 working hours per year was utilized. Based on the experiments conducted at 100 A m^{-2} with a target of 1M NaOH the Specific Productivity was on average 265 kg m^{-2} y^{-1}.

Fig. 13 shows the results obtained for the three investigated scenarios A, B, and C when applying a current density of 300 A m^{-2}. Initial solutions of demineralized water were used for the acid and base inputs.

As is clear from the graph (Fig. 13a), the use of a higher current density allowed the dissociation rate of the water and the consequent production of acid and base to increase, thus resulting in a shorter process time. The yield (Fig. 13b) achieved at the NaOH target value was identical to the yields of the experiments carried out at 100 A m^{-2}. This is because the initial Na^+ ion concentrations, as well as the target concentration, were the same. The same yield value was achieved in a shorter time due to the higher applied current. In principle, tripling the current to 300 A m^{-2} should give a process time equal to one third of the time at 100 A m^{-2}. Contrastingly, the time required was found to be 90, 84, and 78 min, for cases A, B, and C, respectively, thus resulting to be less than a third compared to the time at 100 A m^{-2}. This phenomenon arose due to the greater efficiency of the unit at high currents. As can be seen in Fig. 13c, the current efficiency was 72.3%, 76.8%, and 82.7% at the target concentration, which is on average 11% greater than those

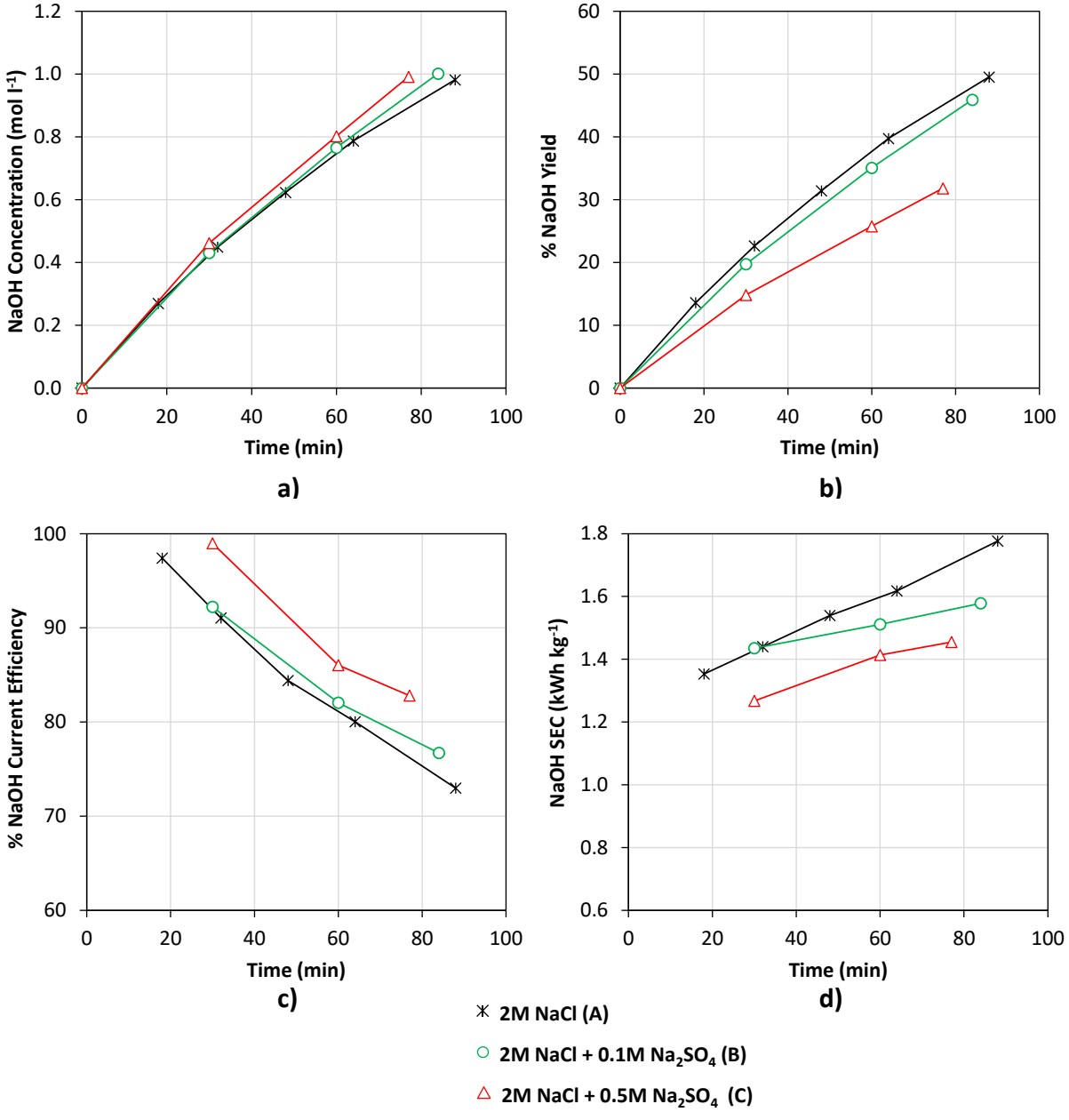

Fig. 13. Time dependency of a) Molar concentration of NaOH, (b) % Yield of NaOH (τ), (c) % Current efficiency of NaOH (η_c) and (d) Specific Energy Consumption of NaOH (*SEC*) as functions of time for a fixed current density of 300 A m^{-2} in a closed-loop configuration. Inlet acid/base compartments: demineralized water.

obtained at a current of 100 A m^{-2}. This was because the diffusive and water fluxes at 300 A m^{-2} had a lower relative weight compared to the migrative flux compared to those at 100 A m^{-2}. The increase in current efficiency should reduce the SEC. However, the higher applied current increases the applied external potential, as a result of the above-mentioned effects of both Nernst potential and ohmic contribution. Accordingly, there was an overall increase in the SEC. The calculated values were 1.79, 1.58, and 1.46 kWh kg^{-1}_{NaOH} for scenarios A, B, and C, respectively, thus making them ~35% higher on average compared with those at 100 A m^{-2} and the same target NaOH concentration.

Finally, on the basis of the experiments conducted at 300 A m^{-2} with the same target, the specific productivity was on average was 923 kg m^{-2} y^{-1}. Therefore, tripling the current density more than tripled the specific productivity. This result is again related to the higher current efficiency obtained at 300 A m^{-2}.

The results presented so far have shown improvements in the performance of the unit when adding sodium sulphate to the EDBM feed. Indeed, when using the same NaOH target there was a reduction in the process time regardless of the applied current. Average increases in current efficiency of 15% and 9.1% were observed at 100 and 300 A m^{-2}, respectively. This caused a significant reduction in the SEC, on average by 18.8%.

Integrating the two units of EFC and EDBM is an innovative solution for minimizing waste brine. The effectiveness of this treatment chain depends not only on the energy consumption of the units but also on the quality of the products obtained, which are NaOH in the base compartment and HCl in the acid compartment for EDBM. In particular, for the two investigated current densities, Table 4 reports the values obtained at the end of the closed-loop tests in terms of the molar fractions of SO_4^{2-} ions in the alkaline and in the acid tanks.

The SO_4^{2-} ions are indicative of the presence of Na_2SO_4 in the base compartment, whereas of H_2SO_4 and Na_2SO_4 in the acid compartment. According to Table 4, the presence of sodium sulphate in the feed caused lower purity of the produced acid and base solutions. In both scenarios B and C, regardless of the applied current density, the % SO_4^{2-} ions in the acid solution was less than 1.2%, whereas this value was less than 0.15% in the base solution, which represents the most valuable product. This shows that the studied unit is very versatile, since changes to the feed do not significantly affect the purity of the obtained products or could even improve the energy performance.

Some recent studies have used EDBM in conjunction with other technologies to recover SWRO brines (Reig et al., 2016a). However, in these works, the EDBM is fed with only NaCl solutions, providing only a limited overview of the proposed technology integrations. Conventional electrodialysis is used in one of these works to pre-concentrate the feed before sending it to the EDBM at concentrations of up to 3.5 M NaCl (Reig et al., 2016b). This enables the production of NaOH (and HCl) concentrations greater than 1M. Increasing the concentration of brine, on the other hand, is inconvenient for a variety of reasons. The first advantage is a decrease in energy consumption. Indeed, according to the results shown in this work (Reig et al., 2016b), the ED unit would increase the specific energy consumption per kg of produced sodium hydroxide by 20% on average. Furthermore, increasing the target concentration of acid and base would result in lower current efficiency due to higher non-ideal phenomena such as diffusion. Additionally, the Nernst potential generated by the pH gradient across the bipolar membranes may increase. As a result, according to Eq. (7), the EDBM unit would have a higher specific energy consumption.

Table 4
% SO_4^{2-} in the acid and base solutions once reached the target concentration.

Current density	Scenario	% SO_4^{2-}	
		Acid	Base
100 A m^{-2}	2M NaCl	–	–
	2M NaCl +0.1M Na_2SO_4	0.25%	0.06%
	2M NaCl +0.5M Na_2SO_4	1.2%	0.15%
300 A m^{-2}	2M NaCl	–	–
	2M NaCl +0.1M Na_2SO_4	0.22%	0.07%
	2M NaCl +0.5M Na_2SO_4	0.77%	~0%

By contrast to other technology integrations in literature, the presence of the EFC unit, as proposed by the present work, would remove the sodium sulphate content from the main feed, thus providing many advantages. Firstly, it would be possible to obtain a pure sodium sulphate salt that could then be sold commercially. Secondly, removing the sodium sulphate would enhance the purity of both the hydrochloric acid and sodium hydroxide solutions, meaning that this could be more easily recirculated into other units of the treatment chain, as recirculation requires purer products. The recirculation, in turn, ensures the circularity of the resources. Higher purity acid and base solutions can also be sold, as the low presence of other chemical species makes them more valuable. In a previous study (Culcasi et al., 2022), it was demonstrated that producing NaOH with EDBM can be less expensive than the chlor-alkali process in terms of Levelized Cost of NaOH (LCoNaOH). However, the output NaOH production from chlor-alkali has a higher concentration ranging from 10 to 30% by weight (Culcasi et al., 2022) compared to the 4% shown in this study. By increasing the applied current density, the concentration of NaOH and HCl can be increased, although at the cost of increasing the SEC. Another possibility is to incorporate an evaporation post-treatment step to increase the outlet concentrations.

Lastly, it would also be possible to produce water that can be used recirculated in the treatment chain, since there is still sodium sulphate in this solution, or be used to pre-cool the feed solution, or be sold, for example, in the fishing industry, demonstrating an additional benefit of the process. In this way, the circular economy of the process can be further ensured.

4. Conclusions

In the present work, an integrated treatment chain comprising both Eutectic Freeze Crystallization and the Electrodialysis with Bipolar Membranes was proposed to recover Na_2SO_4, NaOH, and HCl. Concerning the results collected; firstly, EFC achieved 70% recovery of $Na_2SO_4 \bullet 10H_2O$ without crystallizing NaCl salt with a purity of ~99.9%. In addition, water was recovered in the form of ice with a purity of 93.3%. Following this, a NaCl rich stream can be obtained and fed to the EDBM unit.

EDBM's once-through tests demonstrated that varying the inlet composition of the feed had only negligible effects on the polarization curves. Closed-loop tests showed that a Specific Energy Consumption of 1.4 kWh kg^{-1}_{NaOH} on average could be obtained when operating at a current density in the interval of 100–300 A m^{-2}. Experiments indicated that lowering the current density reduces current efficiency while lowering the Specific Energy Consumption. Interestingly, despite the fact that sulphate in the EDBM feed reduced the purity of the products by 0.34% on average, it produced an average SEC reduction of 19%.

These findings demonstrated the efficacy of this treatment chain, which provides numerous advantages. Both high purity sodium sulphate salt, and acid and base solutions can be obtained and potentially sold. These acid/base could also be recirculated back into the process. Besides the chemicals, desalinated water can also be produced, which increases the water efficiency of the seawater desalination process. Concluding, the integration of EFC and EDBM should be considered as a valid treatment chain to increase the resource recovery for the implementation of a circular desalination system.

CRediT authorship contribution statement

A. Culcasi: Conceptualization, Methodology, Investigation, Validation, Formal analysis, Data curation, Writing – original draft, Visualization. **R. Ktori:** Conceptualization, Methodology, Investigation,

Validation, Formal analysis, Data curation, Writing – original draft, Visualization. **A. Pellegrino:** Formal analysis, Investigation. **M. Rodriguez-Pascual:** Conceptualization, Methodology, Validation, Resources, Writing – review & editing, Supervision. **M.C.M. van Loosdrecht:** Conceptualization, Writing – review & editing, Project administration, Supervision. **A. Tamburini:** Conceptualization, Methodology, Validation, Resources, Writing – review & editing, Supervision. **A. Cipollina:** Conceptualization, Methodology, Validation, Resources, Writing – review & editing, Supervision. **D. Xevgenos:** Conceptualization, Resources, Writing – review & editing, Resources, Supervision, Project administration, Funding acquisition. **G. Micale:** Conceptualization, Methodology, Validation, Resources, Writing – review & editing, Supervision, Project administration.

Declaration of competing interest

The authors declare that they have no known competing financial interests or personal relationships that could have appeared to influence the work reported in this paper.

Acknowledgments

The present work has been carried out thanks to the funding from the European Union's Horizon 2020 research and innovation programme under Grant Agreement no. 869474 (WATER-MINING – Next generation water-smart management systems: large scale demonstrations for a circular economy and society). www.watermining.eu.

Appendix A. Supplementary data

Supplementary data to this article can be found online at https://doi.org/10.1016/j.jclepro.2022.133143.

References

Ahmed, M., Kumar, R., Garudachari, B., Thomas, J.P., 2019. Performance evaluation of a thermoresponsive polyelectrolyte draw solution in a pilot scale forward osmosis seawater desalination system. Desalination 452, 132–140. https://doi.org/10.1016/j.desal.2018.11.013.

Avramidi, E., Gomez Garcia, S., Papaspyrou, S., Louca, V., Xevgenos, Dimitrios, Küpper, F.C., 2022. Benthic biodiversity at the brine discharge sites in the Port of Rotterdam. Water Resour. Ind. 27 https://doi.org/10.1016/j.wri.2022.100173.

Becheleni, E.M.A., Rodriguez-Pascual, M., Lewis, A.E., Rocha, S.D.F., 2017. Influence of phenol on the crystallization kinetics and quality of ice and sodium sulfate decahydrate during eutectic freeze crystallization. Ind. Eng. Chem. Res. 56, 11926–11935. https://doi.org/10.1021/acs.iecr.7b02668.

Campione, A., Gurreri, L., Ciofalo, M., Micale, G., Tamburini, A., Cipollina, A., 2018. Electrodialysis for water desalination: a critical assessment of recent developments on process fundamentals, models and applications. Desalination 434, 121–160. https://doi.org/10.1016/j.desal.2017.12.044.

Culcaci, A., Gurreri, I., Zaffora, A., Cosenza, A., Tamburini, A., Cipollina, A., Micale, G., 2020a. Ionic shortcut currents via manifolds in reverse electrodialysis stacks. Desalination 485. https://doi.org/10.1016/j.desal.2020.114450.

Culcasi, A., Gurreri, L., Cipollina, A., Tamburini, A., Micale, G., 2022. A comprehensive multi-scale model for bipolar membrane electrodialysis (BMED). Chem. Eng. J. 437, 135317 https://doi.org/10.1016/j.cej.2022.135317.

Culcasi, A., Gurreri, L., Zaffora, A., Cosenza, A., Tamburini, A., Micale, G., 2020. On the modelling of an Acid/Base Flow Battery: an innovative electrical energy storage device based on pH and salinity gradients. Appl. Energy 277, 115576. https://doi.org/10.1016/j.apenergy.2020.115576.

Du, F., Warsinger, D.M., Urmi, T.I., Thiel, G.P., Kumar, A., Lienhard, J.H., 2018. Sodium hydroxide production from seawater desalination brine: process design and energy efficiency. Environ. Sci. Technol. 52, 5949–5958. https://doi.org/10.1021/acs.est.8b01195.

Galama, A.H., Post, J.W., Cohen Stuart, M.A., Biesheuvel, P.M., 2013. Validity of the Boltzmann equation to describe Donnan equilibrium at the membrane–solution interface. J. Membr. Sci. 442, 131–139. https://doi.org/10.1016/j.memsci.2013.04.022.

Herrero-Gonzalez, M., Diaz-Guridi, P., Dominguez-Ramos, A., Irabien, A., Ibañez, R., 2020. Highly concentrated HCl and NaOH from brines using electrodialysis with bipolar membranes. Separ. Purif. Technol. 242, 116785 https://doi.org/10.1016/j.seppur.2020.116785.

Heydenrych, H., Pascual, M.R., Lewis, A., 2018. Continuous Eutectic Freeze Crystalliation.

Huang, C., Xu, T., 2006. Electrodialysis with bipolar membranes for sustainable development. Environ. Sci. Technol. 40, 5233–5243. https://doi.org/10.1021/es060039p.

Lassesson, H., Malovanyy, A., Andersson, A., 2021. Optimizing resource flow of industrial processes, with a case study of zero liquid discharge at a copper smelting plant. J. Clean. Prod. 286, 125452 https://doi.org/10.1016/j.jclepro.2020.125452.

Lewis, A., Seckler, M.M., Kramer, H., van Rosmalen, G., 2015. Industrial Crystallization, Industrial Crystallization: Fundamentals and Applications. Cambridge University Press, Cambridge. https://doi.org/10.1017/CBO9781107280427.

Ma, H.P., Wang, H.L., Tian, C.C., Chang, Y.L., Yuan, W., Qi, Y.H., Chao, Z.L., Chen, W.Y., Lv, W.J., 2021. An optimized design for zero liquid discharge from coal chemical industry: a case study in China. J. Clean. Prod. 319, 128572 https://doi.org/10.1016/j.jclepro.2021.128572.

Madaeni, S.S., Mansourpanah, Y., 2004. Chemical cleaning of reverse osmosis membranes fouled by whey. Desalination 161, 13–24. https://doi.org/10.1016/S0011-9164(04)90036-7.

Micari, M., Moser, M., Cipollina, A., Tamburini, A., Micale, G., Bertsch, V., 2020. Towards the implementation of circular economy in the water softening industry: a technical, economic and environmental analysis. J. Clean. Prod. 255, 120291 https://doi.org/10.1016/j.jclepro.2020.120291.

Molinari, R., Avci, A.H., Argurio, P., Curcio, E., Meca, S., Plà-Castellana, M., Cortina, J.L., 2021. Selective precipitation of calcium ion from seawater desalination reverse osmosis brine. J. Clean. Prod. 328, 129645 https://doi.org/10.1016/j.jclepro.2021.129645.

Nima Yazdanpanah, Z.K.N., 2020. The Handbook of Continuous Crystallization. Royal Society of Chemistry, Cambridge. https://doi.org/10.1039/9781788013581.

Panagopoulos, A., 2020. Techno-economic evaluation of a solar multi-effect distillation/thermal vapor compression hybrid system for brine treatment and salt recovery. Chem. Eng. Process. - Process Intensif. 152, 107934 https://doi.org/10.1016/j.cep.2020.107934.

Panagopoulos, A., Haralambous, K.-J., 2020a. Minimal Liquid Discharge (MLD) and Zero Liquid Discharge (ZLD) strategies for wastewater management and resource recovery – analysis, challenges and prospects. J. Environ. Chem. Eng. 8, 104418 https://doi.org/10.1016/j.jece.2020.104418.

Panagopoulos, A., Haralambous, K.-J., Loizidou, M., 2019. Desalination brine disposal methods and treatment technologies - a review. Sci. Total Environ. 693, 133545 https://doi.org/10.1016/j.scitotenv.2019.07.351.

Panagopoulos, A., Haralambous, K.J., 2020b. Minimal Liquid Discharge (MLD) and Zero Liquid Discharge (ZLD) strategies for wastewater management and resource recovery-Analysis, challenges and prospects. J. Environ. Chem. Eng. 8, 104418 https://doi.org/10.1016/j.jece.2020.104418.

Petrik, L.F., Ngo, H., Varjani, S., Osseweijer, P., Xevgenos, D., van Loosdrecht, M., Smol, M., Yang, X., Mateo-Sagasta, J., 2022. From wastewater to resource. One Earth 5, 122–125. https://doi.org/10.1016/j.oneear.2022.01.011.

Prihasto, N., Liu, Q.-F., Kim, S.-H., 2009. Pre-treatment strategies for seawater desalination by reverse osmosis system. Desalination 249, 308–316. https://doi.org/10.1016/j.desal.2008.09.010.

Randall, D.G., Nathoo, J., 2018. Resource recovery by freezing: a thermodynamic comparison between a reverse osmosis brine, seawater and stored urine. J. Water Proc. Eng. 26, 242–249. https://doi.org/10.1016/j.jwpe.2018.10.020.

Randall, D.G., Nathoo, J., Lewis, A.E., 2011. A case study for treating a reverse osmosis brine using Eutectic Freeze Crystallization—Approaching a zero waste process. Desalination 266, 256–262. https://doi.org/10.1016/j.desal.2010.08.034.

Randall, D.G., Zinn, C., Lewis, A.E., 2014. Treatment of textile wastewaters using eutectic freeze crystallization. Water Sci. Technol. 70, 736–741. https://doi.org/10.2166/wst.2014.289.

Reddy, S.T., Lewis, A.E., Witkamp, G.J., Kramer, H.J.M., van Spronsen, J., 2010. Recovery of Na2SO4·10H2O from a reverse osmosis retentate by eutectic freeze crystallisation technology. Chem. Eng. Res. Des. 88, 1153–1157. https://doi.org/10.1016/j.cherd.2010.01.010.

Reig, M., Casas, S., Gibert, O., Valderrama, C., Cortina, J.L., 2016a. Integration of nanofiltration and bipolar electrodialysis for valorization of seawater desalination brines: production of drinking and waste water treatment chemicals. Desalination 382, 13–20. https://doi.org/10.1016/j.desal.2015.12.013.

Reig, M., Casas, S., Valderrama, C., Gibert, O., Cortina, J.L., 2016b. Integration of monopolar and bipolar electrodialysis for valorization of seawater reverse osmosis desalination brines: production of strong acid and base. Desalination 398, 87–97. https://doi.org/10.1016/j.desal.2016.07.024.

Salvador Cob, S., Genceli Güner, F.E., Hofs, B., van Spronsen, J., Witkamp, G.J., 2014. Three strategies to treat reverse osmosis brine and cation exchange spent regenerant to increase system recovery. Desalination 344, 36–47. https://doi.org/10.1016/j.desal.2014.03.009.

Semblante, G.U., Lee, J.Z., Lee, L.Y., Ong, S.L., Ng, H.Y., 2018. Brine pre-treatment technologies for zero liquid discharge systems. Desalination 441, 96–111. https://doi.org/10.1016/j.desal.2018.04.006.

Shahzad, M.W., Burhan, M., Ang, L., Ng, K.C., 2017. Energy-water-environment nexus underpinning future desalination sustainability. Desalination 413, 52–64. https://doi.org/10.1016/j.desal.2017.03.009.

Tong, T., Elimelech, M., 2016. The global rise of zero liquid discharge for wastewater management: drivers, technologies, and future directions. Environ. Sci. Technol. 50, 6846–6855. https://doi.org/10.1021/acs.est.6b01000.

Tsalidis, G.A., Panteleaki Tourkodimitri, K., Mitko, K., Gzyl, G., Skalny, A., Posada, J., Xevgenos, D., 2022. Assessing the environmental performance of a novel coal mine brine treatment technique: A case in Poland. J. Clean. Prod. 358 https://doi.org/10.1016/j.jclepro.2022.131973.

Wang, X., Huang, W., Liu, F., Liu, N., Huang, X., 2018. Determination and graphics expression of ice-salt eutectic points of the multicomponent electrolyte solutions. Fluid Phase Equil. 458, 115–122. https://doi.org/10.1016/j.fluid.2017.10.009.

Xevgenos, D., Argyrou, M., Marcou, M., Louca, V., Mortou, M., Kuepper, F., 2021. Seawater desalination in view of marine environmental and climate change impacts: the case study of Cyprus. Desalination Water Treat. 211 (1), 15–30. https://doi.org/10.5004/dwt.2021.26916.

Xevgenos, Dimitrios, Michailidis, P., Dimopoulos, Konstantinos, Krokida, M., Loizidou, M., 2015a. Design of an innovative vacuum evaporator system for brine concentration assisted by software tool simulation. Desalination Water Treat. 53 (12), 3407–3417. https://doi.org/10.1080/19443994.2014.948660.

Xevgenos, Dimitrios, Vidalis, A., Moustakas, Konstantinos, Malamis, Dimitris, Loizidou, Maria, 2015b. Sustainable management of brine effluent from desalination plants: the SOL-BRINE system. Desalination Water Treat. 53 (12), 3151–3160. https://doi.org/10.1080/19443994.2014.933621.